TISSUE ENGINEERING: Part A
Volume 20, Numbers 15 and 16, 2014

DOI: 10.1089/ten.tea.2013.0523

Adipose-Derived Stem Cells and BMP-2 Delivery in Chitosan-Based 3D Constructs to Enhance Bone Regeneration in a Rat Mandibular Defect Model

Jiabing Fan, MD, PhD,[1,*] Hyejin Park, BS,[1,*] Matthew K. Lee, MD,[2] Olga Bezouglaia, BS,[3] Armita Fartash, BS,[3] Jinku Kim, PhD,[4] Tara Aghaloo, DDS, MD, PhD,[3,†] and Min Lee, PhD[1,5,†]

Reconstructing segmental mandiblular defects remains a challenge in the clinic. Tissue engineering strategies provide an alternative option to resolve this problem. The objective of the present study was to determine the effects of adipose-derived stem cells (ASCs) and bone morphogenetic proteins-2 (BMP-2) in three-dimensional (3D) scaffolds on mandibular repair in a small animal model. *Noggin* expression levels in ASCs were down-regulated by a lentiviral short hairpin RNA strategy to enhance ASC osteogenesis ($ASCs^{Nog-}$). Chitosan (CH) and chondroitin sulfate (CS), natural polysaccharides, were fabricated into 3D porous scaffolds, which were further modified with apatite coatings for enhanced cellular responses and efficient delivery of BMP-2. The efficacy of 3D apatite-coated CH/CS scaffolds supplemented with $ASCs^{Nog-}$ and BMP-2 were evaluated in a rat critical-sized mandibular defect model. After 8 weeks postimplantation, the scaffolds treated with $ASCs^{Nog-}$ and BMP-2 significantly promoted rat mandibular regeneration as demonstrated by micro-computerized tomography, histology, and immunohistochemistry, compared with the groups treated with $ASCs^{Nog-}$ or BMP-2 alone. These results suggest that our combinatorial strategy of $ASCs^{Nog-}$ + BMP-2 in 3D apatite microenvironments can significantly promote mandibular regeneration, and these may provide a potential tissue engineering approach to repair large bony defects.

Introduction

Segmental mandibular defects often result from trauma, infection, dysfunction skeletal development, or secondary treatment of various pathologies such as tumor resection, and severely affect oral functions such as eating and communicating.[1,2] The primary reconstructive repair for mandibular defects requires a free vascularized bone graft. However, this approach requires lengthy surgeries carrying high rates of perioperative complications, such as donor site morbidity.[3] An alternative reconstruction strategy is needed to circumvent associated complications and morbidity associated with standard therapy.[4] Recently, tissue engineering has been exploited as a promising strategy to treat bone defects, utilizing three-dimensional (3D) scaffolds, growth factors, and/or progenitor cells such as mesenchymal stem cells (MSCs).[5]

Cell-based bone tissue engineering strategies are thought to be an attractive option to improve bone repair.[4] MSCs from bone marrow, and adipose and synovial tissue, retain their properties of self-renewal and differentiation into various cell lineages.[6–8] In particular, MSCs isolated from adipose tissue are easily harvested, high proliferative, can differentiate into multiple lineages, and are considered excellent candidates for bone regeneration.[9–11] However, adipose-derived stem cells (ASCs) alone have enjoyed only limited successes in large rat femoral bone defects.[12–14] Human recombinant bone morphogenetic proteins-2 (BMP-2) is a potent osteoinductive factor that has been used with ASCs to enhance bone regeneration.[10] However, high BMP-2

[1]Division of Advanced Prosthodontics, UCLA School of Dentistry, Los Angeles, California.
[2]Department of Head and Neck Surgery, University of California, Los Angeles, Los Angeles, California.
[3]Division of Diagnostic and Surgical Sciences, UCLA School of Dentistry, Los Angeles, California.
[4]Department of Bio and Chemical Engineering, Hongik University, Sejong, Korea.
[5]Department of Bioengineering, University of California, Los Angeles, Los Angeles, California.
*Co-first authors.
†Co-senior authors.

doses, are clinically required for effective bone growth, and such supraphysiological doses may cause serious side effects (e.g., cancer risk).[15]

We recently developed chitosan (CH)-based composite scaffolds that promote osteogenic differentiation of MSCs and protein delivery in a controlled manner with biomimetic apatite on their surfaces.[16] CH is a naturally derived polysaccharide that has been applied to many pharmaceutical and biomedical applications.[17–19] In addition to biocompatibility, CH retains degradation characteristics via enzymatic hydrolysis *in vivo*.[20] Chondroitin sulfate (CS) has been incorporated into CH scaffolds to improve their mechanical properties and biological responses (e.g., cell–material interactions).[16] Furthermore, biomimetic apatite was successfully introduced onto various biomaterial surfaces, such as poly(lactic-co-glycolic acid) (PLGA), tricalcium phosphate (TCP), and CH, for promoting osteogenic activities of progenitor cells and releasing loaded proteins with a reduced initial burst.[21–25]

A number of previous studies demonstrated that reduction of noggin, identified as a BMP signaling inhibitory protein, can significantly enhance osteogenic differentiation of MSCs both *in vitro* and *in vivo*.[26–28] In addition, co-delivery of noggin siRNA and BMP-2 synergistically increased osteogenic differentiation of ASCs *in vitro*.[29] These data suggest that cellular therapy in combination with manipulating BMP signaling antagonists (e.g., noggin) and agonists (e.g., BMP-2), as well as appropriate carriers can have synergistic (or additive) effects on bone regeneration in challenging healing environments. Our recent study revealed that controlled BMP-2 delivery can be achieved by apatite-coated CH-based scaffolds, and BMP-2-loaded scaffolds enhance noggin-suppressed ASC osteogenesis *in vitro*.[25] Furthermore, we have successfully established a novel small animal-model with a mandibular critical-sized defect (CSD) that will not heal spontaneously.[1,3]

In the present study, we evaluated bone regeneration in a rat mandibular CSD model using 3D CH/CS scaffolds in combination with noggin-suppressed ASCs and BMP-2. *Noggin* was downregulated in ASCs by transducing lentivirus particles with short hairpin RNA (shRNA) targeting noggin ($ASCs^{Nog-}$). The scaffolds composed of CH, CS, and apatite on their surfaces were fabricated to slowly release BMP-2. The *in vivo* osteogenic capacity of BMP-2-loaded scaffolds seeded with $ASCs^{Nog-}$ was evaluated in a rat mandibular defect.

Materials and Methods

CH (Mw 255,000, 75%–85% deacetylated), CS sodium salt (Mw 50,000, ≥60% type A) from bovine trachea Collagenase I, and pentasodium tripolyphosphate (TPP) were purchased from Sigma-Aldrich (St. Louis, MO). BMP-2 and ELISA assay kit were purchased from R&D Systems (Minneapolis, MN). Dulbecco's modified Eagle's medium (DMEM), fetal bovine serum (FBS), penicillin/streptomycin (P/S), Live/Dead assay, alamarBlue assay kit, and Alexa fluor-488 goat anti-rabbit IgG antibody were purchased from Life Technologies (Grand Island, NY). C57/BL mice and athymic nude rats were purchased from Charles River Laboratories (Wilmington, MA). Lentiviral particles containing shRNA targeting noggin were purchased from Santa Cruz Biotechnology (Santa Cruz, CA).

Cell harvest

ASCs were isolated from inguinal fat pads in C57BL/6 mice at age of 4–8 weeks according to methods previously described.[7] Briefly, adipose tissues were collected and washed in sterilized phosphate-buffered saline (PBS), cut into small pieces and digested with collagenase type I with a concentration of 0.1% for 2 h. Cells from the digested solution were obtained by centrifugation at 1200 rpm for 5 min, and then resuspended in complete medium containing DMEM, 10% FBS, and 100 U/mL P/S. The resuspended cells were seeded onto tissue culture flasks. The cells at passage 4 were used for the experiments.

Cells transfection

Cells were infected using lentiviral particles containing shRNA targeting noggin according to manufacturer's protocols. Briefly, ASCs at passage 4 were seeded onto six-well culture plates. When cells arrived at 50% confluence after 24 h the growth medium was changed into medium containing lentiviral particles with 8 μg/mL of polybrene. Stable cell clones expressing shRNA were selected using puromycin dihydrochloride.

Preparation of CH-based scaffold

The methods for preparing CH-based scaffolds were described previously.[16] Briefly, CH solution (4.5% w/v) in acetic acid (1 N) was mixed with CS solution (9% w/v) at a ratio of 2:1 (v/v) to obtain CH/CS mixture solution (3% CH/3% CS). The mixed solution was poured into a Petri dish with 2 mm thickness, frozen at −80°C, and then lyophilized in a freeze dryer (Labconco, Kansas City, MO). The obtained CH/CS scaffolds were neutralized by immersing them into NaOH (1 N) for 1 h, and further cross-linked with TPP solution (5% w/v) for 30 min. The cross-linked scaffolds were then washed with ddH_2O, sterilized by immersing them into 70% ethanol for 30 min, and lyophilized. Finally, the obtained scaffolds were cut into a dimension of 5×5 mm for further studies.

Biomimetic apatite coating process

Apatite coating solution was prepared following the methods previously described with some modifications.[30,31] Briefly, simulated body fluids 1 (SBF 1) were prepared by sequentially dissolving $CaCl_2$, $MgCl_2 \cdot 6H_2O$, $NaHCO_3$, and $K_2HPO_4 \cdot 3H_2O$ into ddH_2O. The solution was adjusted to pH 6.0 and then Na_2SO_4, KCl, and NaCl were added. The final solution was adjusted to pH 6.5. Mg^{2+} and HCO_3^- free SBF (SBF 2) was prepared by subsequently dissolving NaCl, $CaCl_2$, and $K_2HPO_4 \cdot 3H_2O$ into ddH_2O and the solution was adjusted to pH 6.4. The obtained scaffolds were subjected to glow discharge argon plasma etching (Harrick Scientific, Ossining, NY). The etched scaffolds were incubated in SBF 1 for 24 h and then changed to SBF 2 for another 24 h at 37°C. The apatite-coated scaffolds were washed with ddH_2O to remove excess ions and lyophilized prior to further studies.

Scanning electron microscopy

The internal morphology of noncoated and coated CH/CS scaffold was examined by scanning electron microscopy

(SEM; Nova Nano SEM 230/FEI, Hillsboro, OR). The cross-sectioned samples were mounted on aluminum stubs and sputter-coated with gold at 20 mA under 70 mTorr for 50 s.

Cell proliferation

$ASCs^{Nog-}$ at passage 8 were seeded onto CH-based scaffolds at a concentration of 3×10^6 cells/mL. The cell/scaffold constructs were cultured in complete DMEM medium containing 10% FBS in 5% CO_2 humidified incubators for up to 21 days. To observe proliferation of the cells cultured on the scaffolds, the cell/scaffold constructs were washed once with PBS and stained with Live/Dead staining kit at 37°C for 20 min. Stained samples were observed under a fluorescence microscope (Olympus, Lake Success, NY) at different time points. Proliferation of cells on the scaffolds was measured using the alamarBlue assay kit. The cell/scaffold constructs at different time points were collected, washed once with PBS, and incubated with sterile alamarBlue solution for 3 h at 37°C. AlamarBlue fluorescence was assayed at 535 nm (excitation) and 600 nm (emission) in plate reader. The experiments were performed in triplicate.

In vitro *release of BMP-2*

BMP-2 release profile in CH-based scaffolds *in vitro* was measured using ELISA assay kit. Briefly, 2.5 μg of BMP-2 in 10 μL PBS with 0.2% bovine serum albumin (BSA) were dropped onto scaffolds at a final concentration of 50 μg/mL. The scaffolds were dried for 15 min under laminar flow and further lyophilized in a freeze dryer for 3 h. The BMP-2 loaded scaffolds were incubated in 1 mL of 10 mM PBS (pH 7.4) at 37°C. The whole incubating solution was removed and replaced with 1 mL fresh solution at predetermined time points over a span of 28 days. The amount of released protein in the supernatant was assayed according to the manufacturer's protocol. The experiment was performed in triplicate, and the amount of protein was released as a percentage of the initial amount of protein loaded.

Rat mandibular defect model

All animals' care and use applied for institutional regulations established and approved by the Animal Research Committee at the University of California, Los Angeles, an AALAC-accredited facility. This study was carried out in strict accordance with the recommendations in the Guide for the Care and Use of Laboratory Animal of the National Institutes of Health.

The critical-size mandible defect (5×5 mm) in athymic nude rats was created according to procedures as previously described.[1] All animals received general anesthesia by inhalational of isoflurane. After hairs on the ventral surface of mandible were shaved, the animals were then prepped and draped according to a sterile manner. An incision overlying and paralleling the left mandible were made using a size #15 blade. The inferior border of the mandible was exposed after deepening down through subcutaneous tissues. The mandible body was further exposed by dissecting the pterygomasseteric sling using electrocautery. The lingual and buccal surfaces of the mandible in a supraperiosteal plane were indentified by bluntly elevating musculature. After measuring 5×5 mm square of mandible defect using a sterilized pen, a 1-mm high-speed cutting burr setting as 3000 rpm, with copious irrigation, was used to remove bone tissue posterior to the incisor and contiguous with the inferior border of the mandible. Hemostasis was attained with electrocautery, and the appropriate size scaffold was placed into the defect using resorbable sutures. The pterygomasseteric sling was then reapproximated using the same resorbable suture and the skin was closed using nonresorbable suture. The experiments were divided into four groups (Table 1). Specifically, apatite-coated CH-based scaffolds ($5\times5\times2$ mm) were fabricated as described in the scaffold preparation above. For BMP-2-loaded scaffolds, 2.5 μg of BMP-2 was adsorbed onto fabricated scaffolds at a final concentration of 50 μg/mL and scaffolds were further lyophilized on a freeze drier for 3 h. Scaffolds were seeded with 2.5×10^5 $ASCs^{Nog-}$ 12 h before implantation. Blank scaffolds were regarded as control group (n = minimum of four rats per group). After surgery, all animals were allowed to recover on warm sheet and then transferred to the vivarium for postoperative care. To get operative treatment, all animals received analgesia with subcutaneous injections of buprenorphine with concentration of 0.1 mg/kg for up to 3 days. To prevent potential infection, all animals also received drinking water including trimethoprim-sulfamethoxazole for up to 7 days.

Table 1. Treatment Groups

Group	*Scaffold volume (μL)*	*BMP-2 dose (μg)*	*Cell number*
Blank scaffold	50	0	0
BMP-2	50	2.5	0
$ASCs^{Nog-}$	50	0	250,000
BMP-2 + $ASCs^{Nog-}$	50	2.5	250,000

ASC, adipose-derived stem cell; BMP-2, bone morphogenetic proteins-2.

3D micro-computerized tomography scanning

After 8 weeks postimplantation, all animals were sacrificed and left mandibles were harvested for analysis. The extracted mandibles were fixed in 4% formaldehyde for 48 h at room temperature with gentle shaking. The fixed samples were rinsed with PBS and then stored with 70% ethanol at 4°C prior to imaging using the high-resolution micro-computerized tomography machine (μCT40; Scanco USA, Inc., Southeastern, PA). The data from the μCT was collected at 50 kVp and 160 μA. Visualization and reconstruction of the data were attained using Dolphin 3D software (Dolphin Imaging & Management Solutions, Chatsworth, CA). Volume analysis of new bone formation was performed using CTAn (Skyscan, Kontich, Belgium). Volume analysis of the specimens included investigations of two volumes and one ratio: bone volume (BV), total volume (TV), and bone volume/total volume (BV/TV). The TV was set as the volume of the original surgical defect that measured $2.5\times5\times5$ mm and was the same across all samples. BV/TV represents the percentage of defect that was healed by new bone tissue.

Histological evaluation

The fixed samples were decalcified under 10% ethylenediaminetetraacetic acid (EDTA) solution under shaking for 3 weeks. The EDTA solution was replaced once every week. Decalcified samples were embedded in paraffin and cut into sections at thickness of 5 μm. The deparaffinzed sections were stained with hematoxylin and eosin (H&E), Sirius red, and Masson's trichrome solution, respectively. Picrosirius red staining solution with a concentration of 0.2% was used to assess collagen expression. Masson's trichrome staining was performed to examine new bone formation. Immunofluorescent staining for osteocalcin (OCN) expression was performed for evaluating active bone formation. The samples were dewaxed and rehydrated, blocked by 2% BSA solution, and then incubated with monoclonal antibodies to OCN (Santa Cruz Biotechnology). A secondary antibody of Alexa fluro-488 goat anti-rabbit IgG was used to develop color. The images for the samples were taken by microscope (Olympus). The collagen and OCN expression was further quantified by image analysis of picrosirus red staining and OCN immuonostaining samples using ImageJ software (NIH, Bethesda, MD) as previously described.[32]

Statistical analysis

Statistical analysis was performed using one way analysis of variances (ANOVA), followed by the Tukey's *post hoc* test. p-Value < 0.05 was considered statistically significant.

Results

Scaffold morphology

The CH/CS composite scaffolds were created as described in our previous studies (Fig. 1).[16] Apatite coating of the obtained CH/CS scaffolds were achieved by immersing scaffolds into SBFs. The apatite coating created on the scaffolds exhibited plate-like morphology (Fig. 1d), while uncoated CH/CS scaffolds have little evidence of this morphology with smooth surfaces (Fig. 1c). The CH/CS scaffolds showed the pore size range from 100 to 150 μm with interconnected porous structures, and the apatite coating did not significantly changed the pore size of the scaffolds.

Cell proliferation on scaffolds

To evaluate the feasibility of CH/CS scaffolds to support cellular proliferation, $ASCs^{Nog-}$ were seeded on the scaffolds and observed by Live/Dead staining (Fig. 2). At day 1, cells remained round morphology on the scaffolds without expansion and they expanded in all groups up to day 21 (Fig. 2a). $ASCs^{Nog-}$ cultured on apatite-coated CH/CS scaffolds appeared to spread greater than cells loaded on uncoated scaffolds at day 21. Proliferation of seeded $ASCs^{Nog-}$ on scaffolds was further studied by an alamarBlue assay (Fig. 2b).

Although there was a trend that the cells proliferated slightly greater on the apatite-coated scaffolds than uncoated scaffolds, there were no statistical differences in cellular proliferation between apatite-coated scaffolds and uncoated scaffolds (Fig. 2b).

Release of BMP-2 from scaffolds

To determine whether apatite coating can reduce initial burst of BMP-2, apatite-coated and uncoated CH/CS scaffolds were loaded with BMP-2 (2.5 μg/scaffold) and the release kinetics of BMP-2 from scaffolds was determined by incubating the scaffolds in PBS. Approximately 35% of initially loaded BMP-2 was released from uncoated scaffold at day 1, while apatite coating significantly reduced the initial burst release of BMP-2 (~18% at day 1) (Fig. 3).

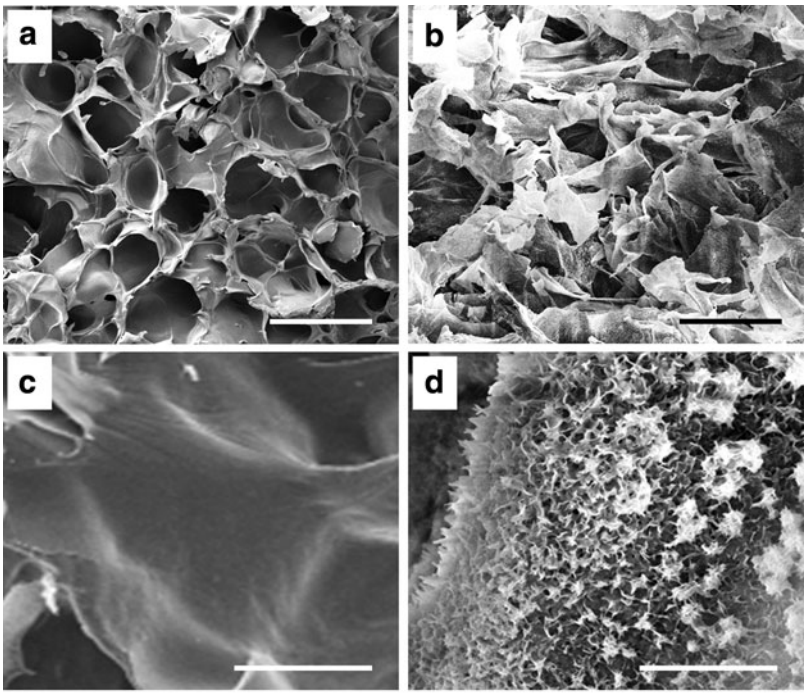

FIG. 1. Scanning electron microscopy images of chitosan (CH)/chondroitin sulfate (CS) scaffolds before **(a, c)** and after **(b, d)** apatite coating: **(a, b)** low magnification. Scale bar = 200 μm; **(c, d)** high magnification. Scale bar = 10 μm.

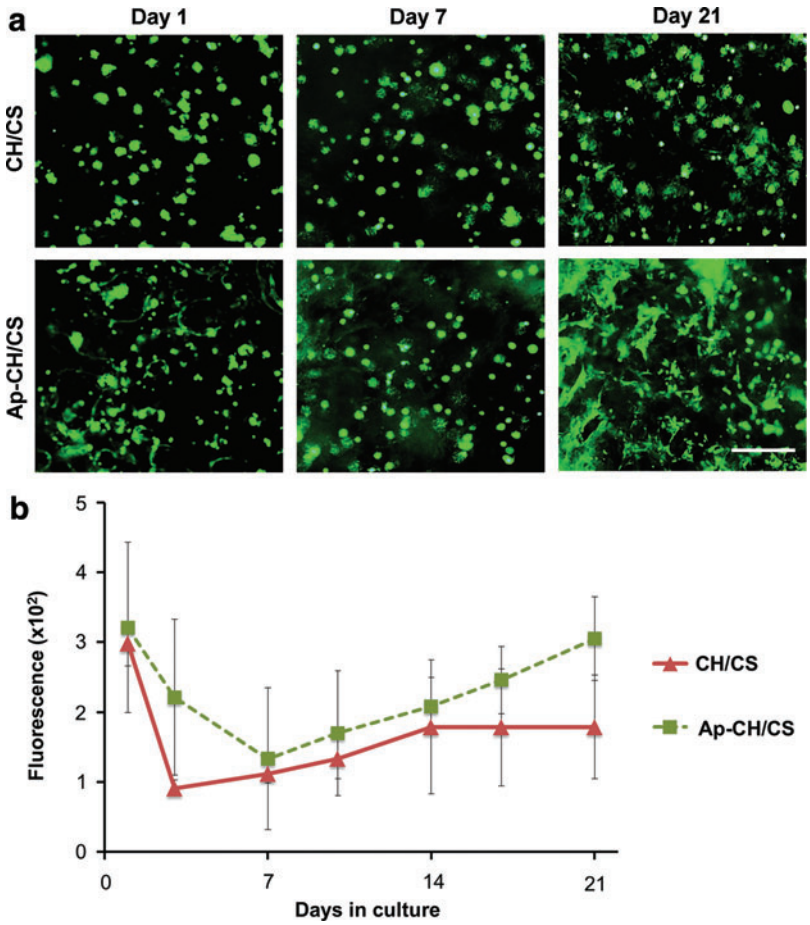

FIG. 2. **(a)** Live/dead fluorescent staining of noggin short hairpin RNA treated adipose-derived stem cells ($ASCs^{Nog-}$) seeded on noncoated (CH/CS) and apatite-coated (Ap-CH/CS) scaffolds after 1, 7, and 21 days in culture. Scale bar = 500 μm. **(b)** Alamar-Blue assay showing proliferation of $ASCs^{Nog-}$ seeded on CH/CS and Ap-CH/CS scaffolds. Color images available online at www.liebertpub.com/tea

Gross observation

Critical-sized marginal mandibular defects (5 × 5 mm) were created in rat mandible (Fig. 4a). The construct of $ASCs^{Nog-}$ and apatite-coated CH/CS scaffold releasing BMP-2 were successfully placed in the created defects (Fig. 4b). During the 8-week period, no infection was detected in all animals. Gross histology of the mandible after sacrifice revealed that the mandibular defects in cell/scaffold group were completely covered by soft tissues and well integrated with the surrounding native mandible (Fig. 4e, f). The defect sites in blank scaffold or BMP-2 carrier alone, however, were morphologically distinct from the surrounding mandible with scaffold-like tissues exposed (Fig. 4c, d).

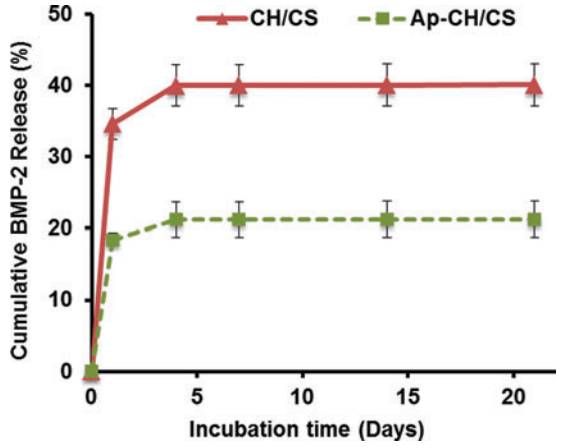

FIG. 3. *In vitro* release of bone morphogenetic proteins-2 (BMP-2) from noncoated (CH/CS) and apatite-coated (Ap-CH/CS) scaffolds evaluated by ELISA assay. Color images available online at www.liebertpub.com/tea

3D μCT analysis

The μCT analysis revealed significantly increased bone formation in the defects implanted with $ASCs^{Nog-}$ + BMP-2 when compared with control (blank scaffold) or defects implanted with $ASCs^{Nog-}$ or BMP-2 alone (Fig. 5). As expected, the defects that were left empty demonstrated no healing up to 8 weeks (data not shown). In particular, there appeared to be more bone formation bridging the defect area implanted with $ASCs^{Nog-}$ + BMP-2 (Fig. 5d) compared with the control group (Fig. 5a). To quantitate the extent of bone formation, the volume of new bone tissue was investigated on postmortem μCT images. Analysis of mandibular defects demonstrated the percentage of new bone formation in the group of $ASCs^{Nog-}$ + BMP-2 delivery was elevated up to 50% greater as compared to that in $ASCs^{Nog-}$ or BMP-2 delivery alone (Fig. 5e). In addition, no significant difference in new bone formation was observed between BMP-2 alone and cell carrier alone, however, each respective treatment group had significantly greater new bone formation (~100% more BV) compared with the control group (Fig. 5e).

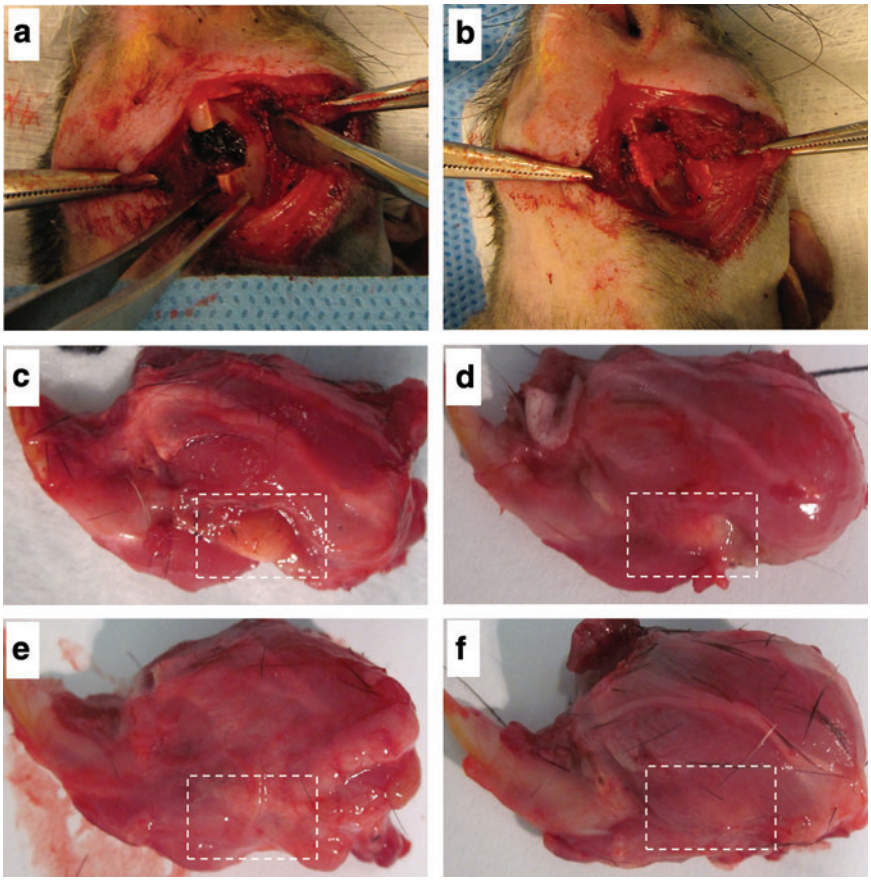

FIG. 4. Mandibular defect model. **(a)** The critical-sized defect (5×5 mm) was created in the left mandible of a rat. **(b)** Ap-CH/CS scaffold loaded with BMP-2, $ASCs^{Nog-}$, or BMP-2 + $ASCs^{Nog-}$ was placed into the defect. Photographs of sacrifice mandibular defects treated with Ap-CH/CS scaffold **(c)**, Ap-CH/CS scaffold loaded with BMP-2 **(d)**, $ASCs^{Nog-}$ **(e)**, or BMP-2 + $ASCs^{Nog-}$ **(f)** at 8 weeks postsurgery. Color images available online at www.liebertpub.com/tea

Histological analysis

Histological evaluation of new bone formation was consistent with μCT findings (Fig. 6). H&E staining at higher magnifications (20× and 40×) revealed a large matured bone formation throughout the mandibular defect area treated with $ASCs^{Nog-}$ + BMP-2 delivery, while no obvious bone formation was found in other groups (Fig. 6). Bone-like tissues were observed in the groups of BMP-2 or $ASCs^{Nog-}$ alone, which were infiltrated by osteoblast-like cells (Fig. 6c). The regenerated bone tissue was further confirmed with Masson's trichrome staining (Fig. 7a). Masson's trichrome staining revealed the presence of mature bone tissues in the group of $ASCs^{Nog-}$ + BMP-2 delivery. Osteoid matrix was observed in the groups of BMP-2 or cell carrier alone, while control groups exhibited fibrous-like tissue with minimal bone formation. Picrosirus red staining was used to examine collagen expression (Fig. 7b, c). Increased collagen deposition was noted in the group of $ASCs^{Nog-}$ + BMP-2 delivery, compared with the control group. To further verify bone formation, we performed immunofluorence staining for OCN, marker for mature bone formation (Fig. 7d). More intense OCN staining was observed in the group of $ASCs^{Nog-}$ + BMP-2 delivery compared with the groups of BMP-2 or cell carrier alone, while OCN expression was scarcely found in the control group. The extent of collagen and OCN expression was further quantitated by image analysis of picrosirus red staining and OCN immuostaining (Fig. 8). Collagen expression in the group of $ASCs^{Nog-}$ + BMP-2 increased up to 12 times, compared with the control group (Fig. 8a). OCN expression significantly elevated up to 66 times in the combination group of $ASCs^{Nog-}$ + BMP-2 when compared with the control group, while there were 30 times increase in BMP-2 or $ASCs^{Nog-}$ alone (Fig. 8b). Quantitation also demonstrated that the combination group had significantly greater expression of the bone markers (i.e., collagen and OCN expression) compared with $ASCs^{Nog-}$ or BMP-2 delivery alone.

Discussion

Human segmental mandibular defects can influence patient's quality of life, which varies with how these defects are reconstructed. Free vascularized bone grafts are considered the gold standard for reconstructing large and complex mandibular defects.[33] However, surgery for free flap transfer is usually associated with high perioperative complication rates, where donor-site morbidity occurs in 30%–40% of patients. These and other complications can occur in more than 60% of elderly patients. Therefore, alternative approaches to treat mandibular defects include tissue engineering strategies.[34]

Small animal models of large mandibular discontinuity defects were not well established and these studies have been done in relatively small through-and-through defects of the mandible because of limited surgical access.[35,36] Recently, our lab established a nonhealing critical-size marginal mandibular defect in a rat model.[1,3] The model created in present study represents clinically relevant mandibular

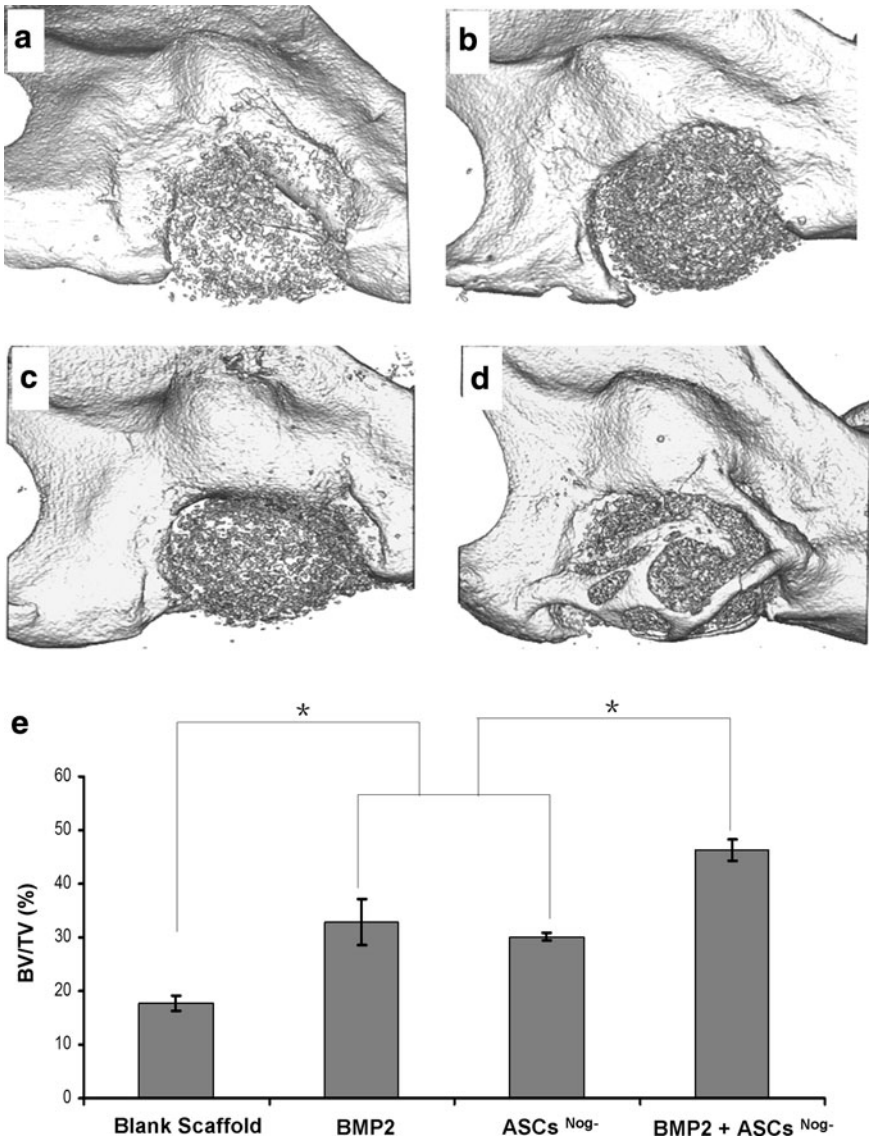

FIG. 5. Micro-computed tomography images of mandibular defects treated with Ap-CH/CS scaffold **(a)**, Ap-CH/CS scaffold loaded with BMP-2 **(b)**, $ASCs^{Nog-}$ **(c)**, or BMP-$2 + ASCs^{Nog-}$ **(d)** at 8 weeks post-surgery. **(e)** Quantification of bone volume/total volume (BV/TV) in mandibular defects.*$p < 0.05$.

defects often created in tumor ablation surgery. We chose this small animal model for its positive financial benefits and ethical implications. However, further standardization of the rat mandible model is necessary besides defect size because the bone healing process can be influenced by many other factors such as rat strain, age, anatomical location, surgical technique, and evaluation method/period.[37]

In the present study, we utilized a tissue engineering approach to repair mandibular bone defects. In particular, CH/CS scaffolds supplemented with BMP-2 and $ASCs^{Nog-}$ enhanced bone regeneration in rat mandibular CSD. We previously developed a biomimetic process to create apatite layers on various biomaterial surfaces (e.g., PLGA, TCP, and CH) and our biomimetic processing strategy resulted in the uniform coating of hydroxyapatite crystalline plates.[16,23–25,30] The created apatite was similar in structure to carbonated hydroxyl apatite prepared under a similar biomimetic process in other studies[38–40] but exhibited different apatite morphology with large plate-like structures. The detailed characterization of the apatite has been described in our previous study.[41] Our present study revealed that apatite coating on CS/CH scaffolds significantly reduced the excessive initial BMP-2 burst release, possibly due to increased electrostatic interaction between positively charged molecules and negatively charged binding sites on the apatite-coated surface.[23] Other studies have indicated that BMP-2 adsorbs on the hydroxyapatite surfaces through electrostatic forces (between the negatively charged carboxylic groups of BMP-2 and the positively charged Ca sites on hydroxyapatites) and water-bridged hydrogen bonds.[42,43] We also speculate that increased surface area from the plate-like morphology of the apatite coating may play a role in reducing initial BMP-2 burst release by increasing retention capacity of the protein. A previous study reported a high correlation between the specific surface area of hydroxyapatite and the adsorbed amount of protein and release kinetics.[44] It was also previously demonstrated that crystallinity, solubility, and surface texture of hydroxyapatite can influence the protein adsorption and release kinetics.[44,45] The final apatite structures can be modulated to achieve the controlled release of protein by regulating various coating process parameters such as ionic strength, pH, and concentration of crystal growth inhibitors in SBF solution.[41,46] Therefore, reducing the initial burst may

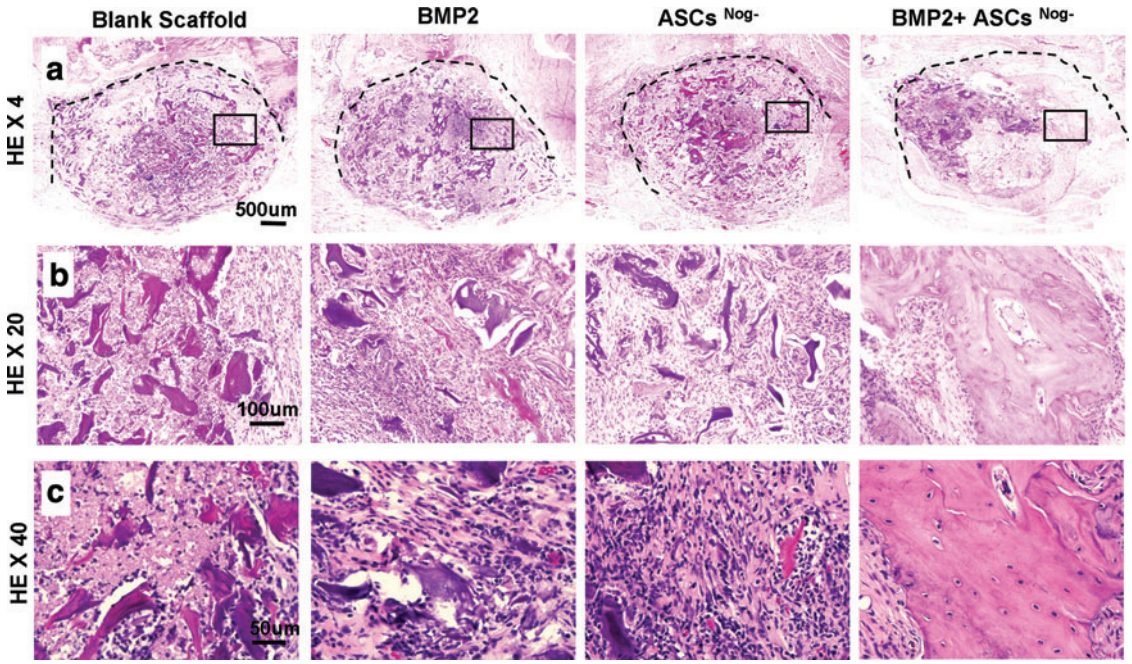

FIG. 6. Hematoxylin-eosin staining of bone formation in mandibular defects treated with Ap-CH/CS scaffold (Blank), Ap-CH/CS scaffold loaded with BMP-2, $ASCs^{Nog-}$, or BMP-2 + $ASCs^{Nog-}$ at 8 weeks postsurgery. Dashed lines indicate approximate margin of defect. Areas within the black boxes are magnified below. Original magnifications: 40× **(a)**; 200× **(b)**; 400× **(c)**. Color images available online at www.liebertpub.com/tea

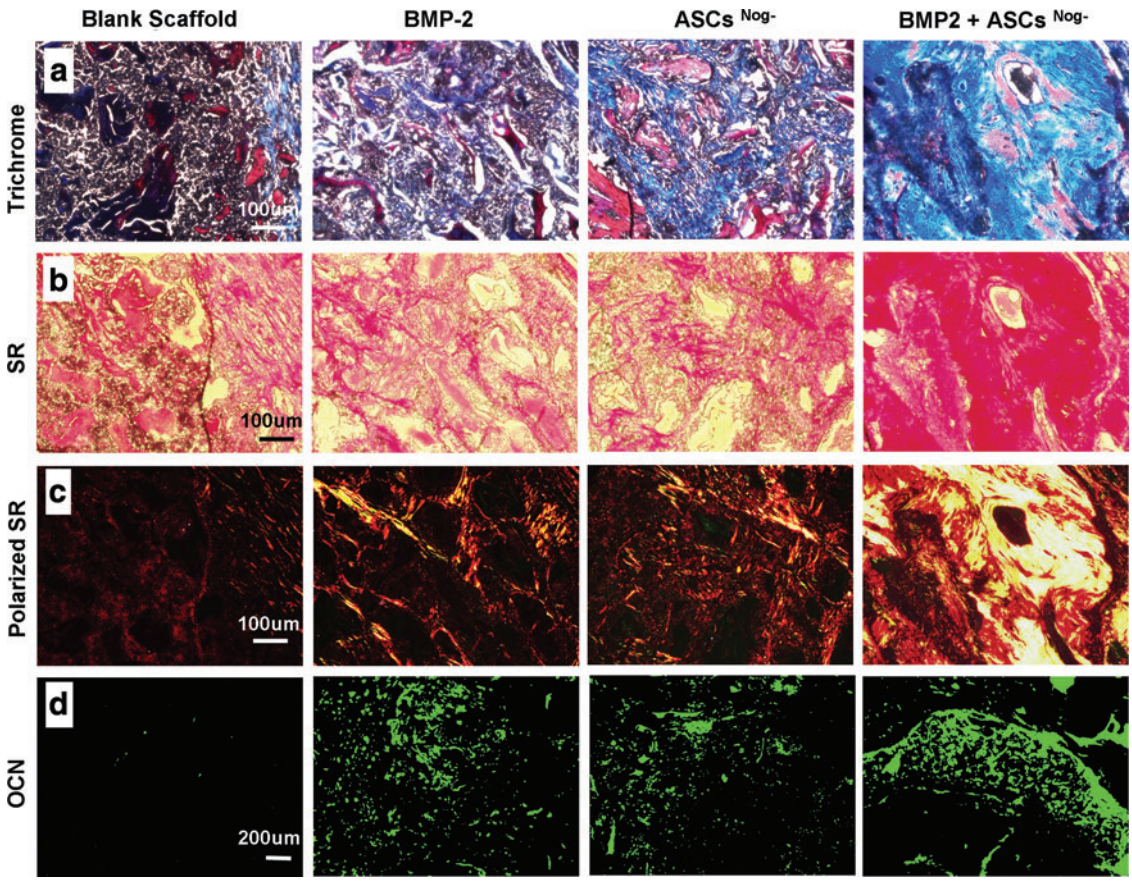

FIG. 7. Histological analysis of bone formation in mandibular defects treated with Ap-CH/CS scaffold (Blank), Ap-CH/CS scaffold loaded with BMP-2, $ASCs^{Nog-}$, or BMP-2 + $ASCs^{Nog-}$ at 8 weeks postsurgery by Masson's trichrome staining **(a)** and sirius red (SR) staining at bright filed **(b)** and polarized light **(c)**. **(d)** Osteocalcin (OCN) immmuofluorescent staining of defect sites. Color images available online at www.liebertpub.com/tea

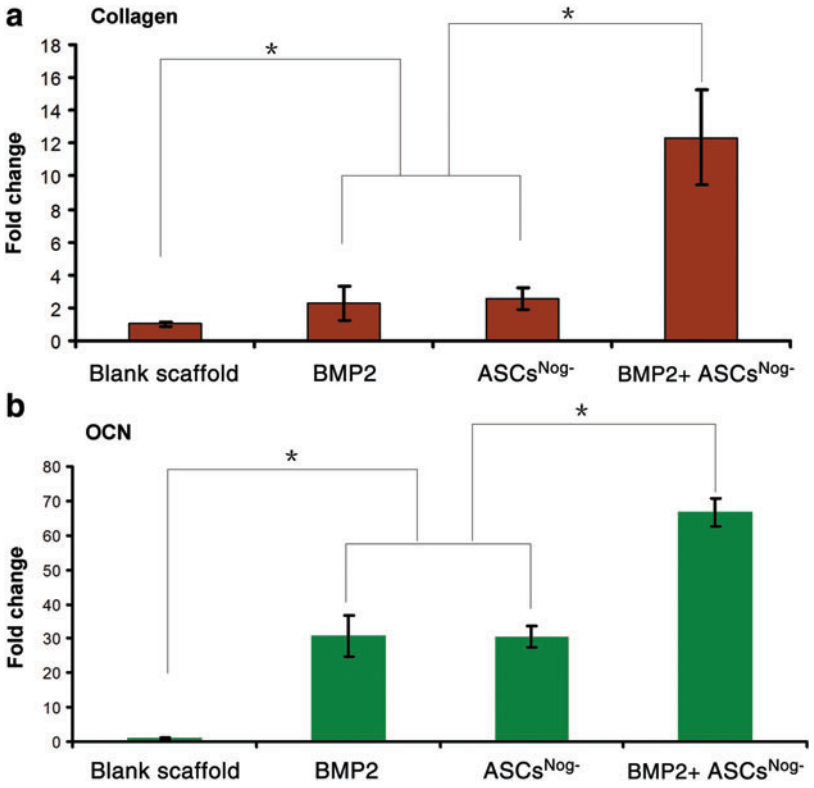

FIG. 8. Relative expression of collagen **(a)** and OCN **(b)** determined by image analysis of sirius red staining and OCN immunofluorescent staining samples. $*p < 0.05$. Color images available online at www.liebertpub.com/tea

prevent adverse side effects such as heterotopic ossification and/or noggin expression resulting from excessive exogenous BMP-2 at the site.[16,27] These data also suggest that apatite coating on CS/CH scaffolds resulted in favorable cellular interactions (e.g., cell spreading and differentiation) of $ASCs^{Nog-}$ on the scaffolds (Fig. 2). Clinical application of ASCs in bone tissue repair possesses several advantages over the use of bone marrow-derived MSCs because of their abundant availability and easy accessibility without painful isolation procedures.[47] Furthermore, BMP-2 stimulated osteogenic differentiation of ASCs. In our previous study, BMP-2 treatment (from 10 to 100 ng/mL) dose-dependently enhanced ALP expression and mineralization in ASCs, which was further increased in noggin-suppressed cells ($ASCs^{Nog-}$).[25] The level of osteogenic differentiation in ASCs treated with BMP-2 (100 ng/mL) was comparable to that of $ASCs^{Nog-}$ treated with 10-fold less BMP-2 (10 ng/mL). These results suggest that suppression of noggin expression in ASCs and simultaneous delivery of BMP-2 in a sustained manner would significantly improve bone formation by increasing BMP activity while reducing dose requirements.

One of the notable findings in this study, as evidenced by histology, was that scaffold degradation may be accelerated by released BMP-2, and thus, provide more space for bone regeneration in the defect. It is possible to assume that BMP-2 released from the carrier may initially attract precursor cells (macrophages and monocytes), which are osteoclast precursors that may explain accelerated scaffold degradation with BMP-2 containing groups.[48,49]

Since 50 μg/mL BMP-2 dose successfully regenerated rat calvarial defects in our previous study,[50] the same final concentration of 50 μg/mL was tested in this rat CSD mandibular model. When standardized for the 5×5-mm mandibular defect volume, this corresponds to a total dose of 2.5 μg. Previous BMP-2 studies for rat mandibular defects applied 10 μg BMP-2 to 2–5 mm diameter defects with ~30% bone healing at 4–8 weeks.[51,52] Other studies used higher BMP-2 dose of 1 mg in a primate model with 20 mm diameter mandible defects and observed minimal bone formation at 16 weeks.[53] Although the results derived from this study will establish the standard for our complementary bone formation strategy of $ASCs^{Nog-}$ + BMP-2 delivery, the effect of BMPs is highly species-specific and the obtained results in rodent models are not necessarily predictive of outcomes in humans. Additional large animal studies are needed for the clinical translation.

Although the current study highlighted the potential of apatite-coated CH-based scaffolds delivering BMP-2 and $ASCs^{Nog-}$ to maximize bone regeneration in the challenging and stringent rat CSD mandibular model, it is also beneficial to use MSCs with noggin suppression in combination with apatite microenvironments derived from this study, without the addition of exogenous growth factors. This strategy would significantly lower costs and potential adverse effects of current BMP therapeutics. Moreover, MSCs are known to elicit immunosuppressive influence that is crucial for preventing graft rejection and inflammation.[54] Hence, the current 3D construct containing MSCs is an effective tissue engineering strategy for bone regeneration.

Overall, the combination of apatite-coated CH/CS scaffold, $ASCs^{Nog-}$ and BMP-2 delivery enhanced bone repair in a rat mandibular defect model compared with the treatment of BMP-2 delivery or $ASCs^{Nog-}$ alone.

Conclusion

CH and CS, naturally occurring polysaccharides, were fabricated into 3D porous scaffolds. Biomimetic apatite

coating promoted robust cell spreading throughout the surface and significantly reduced initial BMP-2 burst release. Bone regeneration in a rat mandibular CSD was maximized when the apatite-coated CH/CS construct was implanted into the defects in combination with $ASCs^{Nog-}$ and BMP-2. The combinatorial strategy of 3D CH-based tissue constructs, $ASCs^{Nog-}$, and BMP-2 provides a promising tissue engineering strategy to promote mandibular regeneration, which will benefit patients with improvements to their quality of life.

Acknowledgments

This work was supported by the National Institutes of Health grants R01 AR060213 and R21 DE021819, the International Association for Dental Research, and the Academy of Osseointegration.

Disclosure Statement

No competing financial interests exist.

References

1. Sidell, D.R., Aghaloo, T., Tetradis, S., Lee, M., Bezouglaia, O., DeConde, A., and St John, M. Composite mandibulectomy: a novel animal model. Otolaryngol Head Neck Surg **146,** 932, 2012.
2. Mikos, A.G., Herring, S.W., Ochareon, P., Elisseeff, J., Lu, H.H., Kandel, R., Schoen, F.J., Toner, M., Mooney, D., Atala, A., Van Dyke, M.E., Kaplan, D., and Vunjak-Novakovic, G. Engineering complex tissues. Tissue Eng **12,** 3307, 2006.
3. DeConde, A.S., Sidell, D., Lee, M., Bezouglaia, O., Low, K., Elashoff, D., Grogan, T., Tetradis, S., Aghaloo, T., and St John, M. Bone morphogenetic protein-2-impregnated biomimetic scaffolds successfully induce bone healing in a marginal mandibular defect. Laryngoscope **123,** 1149, 2013.
4. Meijer, G.J., de Bruijn, J.D., Koole, R., and van Blitterswijk, C.A. Cell-based bone tissue engineering. PLoS Med **4,** 260, 2007.
5. Khan, Y., Yaszemski, M.J., Mikos, A.G., and Laurencin, C.T. Tissue engineering of bone: material and matrix considerations. J Bone Joint Surg Am **90A,** 36, 2008.
6. Pittenger, M.F., Mackay, A.M., Beck, S.C., Jaiswal, R.K., Douglas, R., Mosca, J.D., Moorman, M.A., Simonetti, D.W., Craig, S., and Marshak, D.R. Multilineage potential of adult human mesenchymal stem cells. Science **284,** 143, 1999.
7. Estes, B.T., Diekman, B.O., Gimble, J.M., and Guilak, F. Isolation of adipose-derived stem cells and their induction to a chondrogenic phenotype. Nat Protoc **5,** 1294, 2010.
8. Fan, J., Varshney, R.R., Ren, L., Cai, D., and Wang, D.A. Synovium-derived mesenchymal stem cells: a new cell source for musculoskeletal regeneration. Tissue Eng Part B Rev **15,** 75, 2009.
9. Zuk, P.A., Zhu, M., Mizuno, H., Huang, J., Futrell, J.W., Katz, A.J., Benhaim, P., Lorenz, H.P., and Hedrick, M.H. Multilineage cells from human adipose tissue: implications for cell-based therapies. Tissue Eng **7,** 211, 2001.
10. Levi, B., James, A.W., Nelson, E.R., Vistnes, D., Wu, B., Lee, M., Gupta, A., and Longaker, M.T. Human adipose derived stromal cells heal critical size mouse calvarial defects. PLoS One **5,** e11177, 2010.
11. Cowan, C.M., Shi, Y.Y., Aalami, O.O., Chou, Y.F., Mari, C., Thomas, R., Quarto, N., Contag, C.H., Wu, B., and Longaker, M.T. Adipose-derived adult stromal cells heal critical-size mouse calvarial defects. Nat Biotechnol **22,** 560, 2004.
12. Chou, Y.F., Zuk, P.A., Chang, T.L., Benhaim, P., and Wu, B.M. Adipose-derived stem cells and BMP2: part 1. BMP2-treated adipose-derived stem cells do not improve repair of segmental femoral defects. Connect Tissue Res **52,** 109, 2011.
13. Jeon, O., Rhie, J.W., Kwon, I.K., Kim, J.H., Kim, B.S., and Lee, S.H. *In vivo* bone formation following transplantation of human adipose-derived stromal cells that are not differentiated osteogenically. Tissue Eng Part A **14,** 1285, 2008.
14. Peterson, B., Zhang, J., Iglesias, R., Kabo, M., Hedrick, M., Benhaim, P., Hedrick, M., Benhaim, P., and Lieberman, J.R. Healing of critically sized femoral defects, using genetically modified mesenchymal stem cells from human adipose tissue. Tissue Eng **11,** 120, 2005.
15. Carragee, E.J., Hurwitz, E.L., and Weiner, B.K. A critical review of recombinant human bone morphogenetic protein-2 trials in spinal surgery: emerging safety concerns and lessons learned. Spine J **11,** 471, 2011.
16. Park, H., Choi, B., Nguyen, J., Fan, J., Shafi, S., Klokkevold, P., and Lee, M. Anionic carbohydrate-containing chitosan scaffolds for bone regeneration. Carbohydr Polym **97,** 587, 2013.
17. Li, Z., Ramay, H.R., Hauch, K.D., Xiao, D., and Zhang, M. Chitosan-alginate hybrid scaffolds for bone tissue engineering. Biomaterials **26,** 3919, 2005.
18. Kumar, M.N., Muzzarelli, R.A., Muzzarelli, C., Sashiwa, H., and Domb, A.J. Chitosan chemistry and pharmaceutical perspectives. Chem Rev **104,** 6017, 2004.
19. Lee, K.Y., and Mooney, D.J. Hydrogels for tissue engineering. Chem Rev **101,** 1869, 2001.
20. Tomihata, K., and Ikada, Y. *In vitro* and *in vivo* degradation of films of chitin and its deacetylated derivatives. Biomaterials **18,** 567, 1997.
21. Kim, S.S., Park, M.S., Jeon, O., Choi, C.Y., and Kim, B.S. Poly(lactide-co-glycolide)/hydroxyapatite composite scaffolds for bone tissue engineering. Biomaterials **27,** 1399, 2006.
22. Kong, L., Gao, Y., Cao, W., Gong, Y., Zhao, N., and Zhang, X. Preparation and characterization of nano-hydroxyapatite/chitosan composite scaffolds. J Biomed Mater Res A **75,** 275, 2005.
23. Lee, M., Li, W., Siu, R.K., Whang, J., Zhang, X., Soo, C., Ting, K., and Wu, B.M. Biomimetic apatite-coated alginate/chitosan microparticles as osteogenic protein carriers. Biomaterials **30,** 6094, 2009.
24. Hu, J., Hou, Y., Park, H., and Lee, M. Beta-tricalcium phosphate particles as a controlled release carrier of osteogenic proteins for bone tissue engineering. J Biomed Mater Res A **100**, 1680, 2012.
25. Fan, J., Park, H., Tan, S., and Lee, M. Enhanced osteogenesis of adipose derived stem cells with noggin suppression and delivery of BMP-2. PLoS One **8,** e72474, 2013.
26. Gazzerro, E., Du, Z., Devlin, R.D., Rydziel, S., Priest, L., Economides, A.N., and Canalis, E. Noggin arrests stromal cell differentiation *in vitro*. Bone **32,** 111, 2003.
27. Gazzerro, E., Gangji, V., and Canalis, E. Bone morphogenetic proteins induce the expression of noggin, which

limits their activity in cultured rat osteoblasts. J Clin Invest **102,** 2106, 1998.
28. Wan, D.C., Pomerantz, J.H., Brunet, L.J., Kim, J.B., Chou, Y.F., Wu, B.M., Harland, R., Blau, H.M., and Longaker, M.T. Noggin suppression enhances *in vitro* osteogenesis and accelerates *in vivo* bone formation. J Biol Chem **282,** 26450, 2007.
29. Ramasubramanian, A., Shiigi, S., Lee, G.K., and Yang, F. Non-viral delivery of inductive and suppressive genes to adipose-derived stem cells for osteogenic differentiation. Pharmaceut Res **28,** 1328, 2011.
30. Chou, Y.F., Dunn, J.C., and Wu, B.M. *In vitro* response of MC3T3-E1 pre-osteoblasts within three-dimensional apatite-coated PLGA scaffolds. J Biomed Mater Res B Appl Biomater **75,** 81, 2005.
31. Chou, Y.F., Huang, W., Dunn, J.C., Miller, T.A., and Wu, B.M. The effect of biomimetic apatite structure on osteoblast viability, proliferation, and gene expression. Biomaterials **26,** 285, 2005.
32. Zhang, D., and Kilian, K.A. The effect of mesenchymal stem cell shape on the maintenance of multipotency. Biomaterials **34,** 3962, 2013.
33. Greenward, A.S., Boden, S.D., Barrak, R.L., Bostrom, M.P.G., Goldberg, V.M., Yaszemski, M.J., and Helm, C.S. The evolving role of bone-graft substitutes. American academy of orthopaedic surgeons *77th Annual Meeting*. New Orleans, LA, 2010.
34. Abukawa, H., Shin, M., Williams, W.B., Vacanti, J.P., Kaban, L.B., and Troulis, M.J. Reconstruction of mandibular defects with autologous tissue-engineered bone. J Oral Maxillofac Surg **62,** 601, 2004.
35. Schliephake, H., Weich, H.A., Dullin, C., Gruber, R., and Frahse, S. Mandibular bone repair by implantation of rhBMP-2 in a slow release carrier of polylactic acid—an experimental study in rats. Biomaterials **29,** 103, 2008.
36. Schmitz, J.P., and Hollinger, J.O. The critical size defect as an experimental model for craniomandibulofacial nonunions. Clin Orthop Relat Res **205,** 299, 1986.
37. Vajgel, A., Mardas, N., Farias, B.C., Petrie, A., Cimões, R., and Donos, N. A systematic review on the critical size defect model. Clin Oral Implants Res 2013. DOI: 10.1111/clr.12194.
38. Leonor, I.B., Baran, E.T., Kawashita, M., Reis, R.L., Kokubo, T., and Nakamura, T. Growth of a bonelike apatite on chitosan microparticles after a calcium silicate treatment. Acta Biomater **4,** 1349, 2008.
39. Du, C., Klasens, P., Haan, R.E., Bezemer, J., Cui, F.Z., de Groot, K., and Layrolle, P. Biomimetic calcium phosphate coatings on Polyactive 1000/70/30. J Biomed Mater Res **59,** 535, 2002.
40. Jayasuriya, A.C., Shah, C., Ebraheim, N.A., and Jayatissa, A.H. Acceleration of biomimetic mineralization to apply in bone regeneration. Biomed Mater **3,** 015003, 2008.
41. Chou, Y.F., Chiou, W.A., Xu, Y., Dunn, J.C., and Wu, B.M. The effect of pH on the structural evolution of accelerated biomimetic apatite. Biomaterials **25,** 5323, 2004.
42. Boix, T., Gómez-Morales, J., Torrent-Burgués, J., Monfort, A., Puigdomènech, P., and Rodríguez-Clemente, R. Adsorption of recombinant human bone morphogenetic protein rhBMP-2m onto hydroxyapatite. J Inorg Biochem **99,** 1043, 2005.
43. Dong, X., Wang, Q., Wu, T., and Pan, H. Understanding adsorption-desorption dynamics of BMP-2 on hydroxyapatite (001) surface. Biophys J **93,** 750, 2007.
44. Matsumoto, T., Okazaki, M., Inoue, M., Yamaguchi, S., Kusunose, T., Toyonaga, T., Hamada, Y., and Takahashi, J. Hydroxyapatite particles as a controlled release carrier of protein. Biomaterials **25,** 3807, 2004.
45. Kandori, K., Shimizu, T., Yasukawa, A., and Ishikawa, T. Adsorption of bovine serum-albumin onto synthetic calcium hydroxyapatite—influence of particle texture. Colloid Surf B **5,** 81, 1995.
46. Barrere, F., van Blitterswijk, C.A., de Groot, K., and Layrolle, P. Influence of ionic strength and carbonate on the Ca-P coating formation from SBFx5 solution. Biomaterials **23,** 1921, 2002.
47. Zhu, M., Heydarkhan-Hagvall, S., Hedrick, M., Benhaim, P., and Zuk, P. Manual isolation of adipose-derived stem cells from human lipoaspirates. J Vis Exp 2013. DOI: 10.3791/50585.
48. Termaat, M.F., Den Boer, F.C., Bakker, F.C., Patka, P., and Haarman, H.J.T.M. Bone morphogenetic proteins—development and clinical efficacy in the treatment of fractures and bone defects. J Bone Joint Surg Am **87A,** 1367, 2005.
49. Bessa, P.C., Casal, M., and Reis, R.L. Bone morphogenetic proteins in tissue engineering: the road from the laboratory to the clinic, part I (basic concepts). J Tissue Eng Regen M **2,** 1, 2008.
50. Aghaloo, T., Cowan, C.M., Chou, Y.F., Zhang, X., Lee, H., Miao, S., Hong, N., Kuroda, S., Wu, B., Ting, K., and Soo, C. Nell-1-induced bone regeneration in calvarial defects. Am J Pathol **169,** 903, 2006.
51. Arosarena, O., and Collins, W. Comparison of BMP-2 and -4 for rat mandibular bone regeneration at various doses. Orthod Craniofac Res **8,** 267, 2005.
52. Wen, B., Karl, M., Pendrys, D., Shafer, D., Freilich, M., and Kuhn, L. An evaluation of BMP-2 delivery from scaffolds with miniaturized dental implants in a novel rat mandible model. J Biomed Mater Res B Appl Biomater **97,** 315, 2011.
53. Seto, I., Asahina, I., Oda, M., and Enomoto, S. Reconstruction of the primate mandible with a combination graft of recombinant human bone morphogenetic protein-2 and bone marrow. J Oral Maxillofac Surg **59,** 53, 2011.
54. Caplan, A.I., and Bruder, S.P. Mesenchymal stem cells: building blocks for molecular medicine in the 21st century. Trends Mol Med **7,** 59, 2001.

Address correspondence to:
Tara Aghaloo, DDS, MD, PhD
Division of Diagnostic and Surgical Sciences
UCLA School of Dentistry
10833 Le Conte Avenue
CHS 53-009
Los Angeles, CA 90095-1668

E-mail: taghaloo@dentistry.ucla.edu

Min Lee, PhD
Division of Advanced Prosthodontics
UCLA School of Dentistry
10833 Le Conte Avenue
CHS 23-032B
Los Angeles, CA 90095-1668

E-mail: leemin@ucla.edu

Received: August 22, 2013
Accepted: February 10, 2014
Online Publication Date: May 9, 2014